NANOSYSTEMS:
PHYSICS, CHEMISTRY, MATHEMATICS

Original article

Chebanenko M.I., et al. *Nanosystems: Phys. Chem. Math.*, 2025, **16** (4), 510–520.
http://nanojournal.ifmo.ru
DOI 10.17586/2220-8054-2025-16-4-510-520

Self-cleaning nanocomposite membranes based on sulfonated tetrafluoroethylene and g-C_3N_4 for water purification

Maria I. Chebanenko[1,a], Lev A. Lebedev[1,b], Maksim I. Tenevich[1,c], Kirill D. Martinson[1,d], Oleg N. Primachenko[2,e], Svetlana V. Kononova[2,f], Vadim I. Popkov[1,g]

[1]Ioffe Institute, St. Petersburg, Russia

[2]Institute of Macromolecular Compounds, St. Petersburg, Russia

[a]m_chebanenko@list.ru, [b]1595lion@gmail.com, [c]chwm420@gmail.com, [d]martinsonkirill@mail.ru, [e]alex-prima@mail.ru, [f]svkononova@list.ru, [g]vadim.i.popkov@mail.ioffe.ru

Corresponding author: M. I. Chebanenko, m_chebanenko@list.ru

PACS 61.43.Gt, 61.46.+w

ABSTRACT Water contamination from industrial effluents is a significant environmental challenge due to the presence of organic dyes. This study presents the development of self-cleaning nanocomposite membranes based on sulfonated tetrafluoroethylene and 2D graphitic carbon nitride (g-C_3N_4) nanosheets for efficient water purification. The membranes were synthesized using solution casting with 1 and 5 wt. % g-C_3N_4 as a photocatalytic filler. A comprehensive physicochemical characterization was conducted using XRD, FTIR, SEM, DRS, and adsorption tests. The photocatalytic performance was assessed through the degradation of methylene blue under visible light. Results show that membranes with 5 wt. % g-C_3N_4 exhibit enhanced adsorption efficiency ($k = 0.0800$ min^{-1}) and notable photocatalytic activity ($k = 0.0083$ min^{-1}), leading to effective dye removal and self-cleaning functionality. These findings highlight the potential of hybrid polymer-nanomaterial membranes for sustainable wastewater treatment. The proposed membranes offer a promising solution for removing hazardous organic pollutants while maintaining long-term operational stability.

KEYWORDS polymers, metal-free catalysts, ionomeric fluoropolymer membranes, smart nanomaterials, photocatalysis, advanced oxidation processes, dye removal, environmental remediation

ACKNOWLEDGEMENTS M. I. Chebanenko, L. A. Lebedev, M. I. Tenevich, K. D. Martinson, and V. I. Popkov from the Ioffe Institute acknowledge support from the Ministry of Science and Higher Education of the Russian Federation under State Assignment No. FFUG-2024-0036. O. N. Primachenko and S. V. Kononova from the Branch of Petersburg Nuclear Physics Institute Named by B. P. Konstantinov of the National Research Centre "Kurchatov Institute" – Institute of Macromolecular Compounds acknowledge support under State Assignment No. 1021062411582-7-1.4.4. The authors acknowledge the use of AI-assisted tools (Grammarly, DeepL Write) solely for language editing purposes. The content, analysis, and conclusions presented in this work are entirely the responsibility of the authors.

FOR CITATION Chebanenko M.I., Lebedev L.A., Tenevich M.I., Martinson K.D., Primachenko O.N., Kononova S.V., Popkov V.I. Self-cleaning nanocomposite membranes based on sulfonated tetrafluoroethylene and g-C_3N_4 for water purification. *Nanosystems: Phys. Chem. Math.*, 2025, **16** (4), 510–520.

1. Introduction

The growing contamination of aquatic ecosystems by industrial effluents has become a critical environmental issue, particularly due to the discharge of synthetic dyes from textile and dyeing industries. These dyes exhibit high chemical stability, low biodegradability, and strong resistance to conventional water treatment processes, leading to their persistent accumulation in water bodies [1–3]. Exposure to such pollutants poses severe ecological and human health risks, necessitating the development of advanced water purification technologies that are both efficient and sustainable.

Traditional treatment methods, including coagulation [4–6], flotation [7,8], adsorption [9,10], and biological degradation [11–13], have been widely employed for wastewater treatment. However, these techniques often suffer from limited efficiency in removing complex organic dyes and require secondary treatments to achieve complete decontamination. In recent years, advanced oxidation processes (AOPs) have emerged as an alternative strategy to overcome these limitations by facilitating the degradation of persistent pollutants through the generation of highly reactive oxidative species [14, 15]. Despite their effectiveness, AOPs require high energy input or chemical consumption, limiting their large-scale application [16].

Consequently, there has been an increasing focus on membrane-based separation technologies, such as microfiltration, ultrafiltration, nanofiltration, and reverse osmosis [17, 18]. These techniques have demonstrated excellent removal

rates for a broad spectrum of contaminants, including heavy metals, organic pollutants, and microbial pathogens [19]. However, despite their advantages, membrane fouling, high operational costs, and frequent membrane replacement remain significant challenges, restricting their long-term sustainability in wastewater treatment applications [20].

To address these limitations, nanostructured materials have been explored as functional additives for enhancing membrane performance. Among them, graphitic carbon nitride (g-C_3N_4) has emerged as a highly promising photocatalytic nanomaterial due to its metal-free composition, tunable bandgap ($\sim$2.7 eV), and visible-light-driven photocatalytic activity [21, 22]. The incorporation of g-C_3N_4 into polymeric membranes enhances their adsorptive and photocatalytic properties, facilitating the degradation of organic pollutants under ambient conditions [23]. Furthermore, the high stability, low toxicity, and cost-effectiveness of g-C_3N_4 make it an attractive candidate for sustainable water purification applications. In addition, photocatalytic coatings based on g-C_3N_4 have been explored for self-cleaning surfaces, which shares common antifouling properties with membrane-based photocatalytic materials [24, 25].

In this study, we present the synthesis and characterization of self-cleaning nanocomposite membranes based on sulfonated tetrafluoroethylene and g-C_3N_4 nanosheets. The research focuses on understanding the synergistic effects of g-C_3N_4 on the physicochemical properties, adsorption capacity, and photocatalytic performance of the membranes. Special emphasis is placed on the degradation of methylene blue (MB) under visible-light irradiation, demonstrating the potential of these membranes for cost-effective and energy-efficient wastewater treatment. The findings contribute to the ongoing development of next-generation smart membranes for advanced water purification [26, 27].

2. Experimental

2.1. Synthesis of powder g-C_3N_4

Powder graphitic carbon nitride (g-C_3N_4) was synthesized via thermal polymerization using urea (CH_4N_2O) as a precursor. The synthesis procedure followed a previously reported method [19]. The obtained sample was designated as CN-IN.

2.2. Preparation of g-C_3N_4-modified membranes

The g-C_3N_4-modified membranes were synthesized using a solution casting method, following the procedure outlined in [28]. A stable polymer dispersion of the ionomer LSC-1, a domestic analog of Nafion with an equivalent weight of 1030 g-equiv/mol, was prepared by dissolving 5.1 wt. % of the copolymer in its sulfonic acid form in dimethylformamide (DMF) at 80 °C under continuous stirring.

To achieve a homogeneous distribution of the g-C_3N_4 nanofiller, its suspension in DMF was subjected to mechanical stirring at 1000 rpm using a top-mounted laboratory mixer, followed by ultrasonic treatment for 30 minutes. The resulting g-C_3N_4 suspension was then mixed with the LSC-1 dispersion at mass ratios of 1 and 5 wt. % relative to the polymer, with additional stirring for 5 minutes to ensure a stable and uniform dispersion.

The final dispersion was poured into a Petri dish and subjected to solvent evaporation under an infrared (IR) lamp for 3 hours until a polymeric membrane was formed. To remove residual solvent, the membrane was subsequently annealed at 100 °C for 3 hours under vacuum. After annealing, the membranes were treated with a 15 % aqueous nitric acid solution, followed by thorough rinsing with distilled water to remove any remaining acid residues.

As a result, membranes containing 0, 1, and 5 wt. % of g-C_3N_4 were obtained and designated as M-IN, M-1 % CN, and M-5 % CN, respectively.

2.3. Structural and morphological characterization

2.3.1. X-Ray Diffraction (XRD) analysis. The phase composition of the synthesized materials was investigated using X-ray diffraction (XRD) on a Rigaku SmartLab 3 diffractometer equipped with CuKα radiation ($\lambda = 0.154051$ nm). Diffraction patterns were recorded over the Bragg angle range of 10 – 80°, and phase identification was performed using the Crystallography Open Database (COD).

2.3.2. Fourier-Transform Infrared Spectroscopy (FTIR). Fourier-transform infrared (FTIR) spectroscopy was conducted using a Shimadzu IRTracer-100 spectrometer equipped with a Specac ATR attachment. Spectra were recorded over the wavenumber range of 350 – 4000 cm^{-1} using a diamond ATR crystal with a penetration depth of approximately 2 μm at a 45° incidence angle.

2.3.3. Scanning Electron Microscopy (SEM) analysis. The morphology of powder g-C_3N_4 powder and the membrane containing 5 wt. % g-C_3N_4 was analyzed using scanning electron microscopy (SEM) with a Tescan Vega 3 SBH microscope equipped with an Oxford INCA energy-dispersive X-ray spectroscopy (EDS) system.

2.3.4. Nitrogen adsorption-desorption isotherms. Textural properties of the powder g-C_3N_4 sample were evaluated via nitrogen adsorption-desorption measurements using a Micromeritics ASAP 2020 Surface Area and Porosity Analyzer. The analysis was conducted at liquid nitrogen temperature (77 K).

2.3.5. Diffuse Reflectance UV-Vis Spectroscopy (DRS). Diffuse reflectance spectra (DRS) were recorded in the wavelength range of 350 – 700 nm using an Avaspec-ULS2048CL-EVO spectrometer equipped with an AvaSphere-30-REFL integrating sphere.

2.4. Adsorption and photocatalytic performance

2.4.1. Adsorption measurement. Methylene blue (MB, $C_{16}H_{18}ClN_3S{\cdot}H_2O$), a cationic organic dye, was used as a model pollutant to evaluate the adsorption capacity of the synthesized membranes. Membrane samples with an area of 1 cm^2 were placed in 4 mL quartz cuvettes containing an MB solution (0.05 g/L). Absorption spectra were recorded at 5-minute intervals using an Avaspec-ULS2048CL-EVO spectrometer equipped with an Avalight-XE pulsed xenon light source.

2.4.2. Photocatalytic degradation test. The photocatalytic activity of the membranes was evaluated based on the degradation of MB under visible light irradiation. For the test, membrane samples (7 mm in diameter) were placed in a sample holder, and 100 μL of MB solution was drop-cast onto their surface. The membranes were then dried at 60 °C before the photocatalytic test. During the experiment, the MB-loaded membranes were kept in a closed reaction chamber and irradiated with visible light-emitting diodes (LEDs, 12 W, $\lambda_{\max} = 405$ nm). Absorption spectra were recorded at 15-minute intervals using an Avaspec-ULS2048CL-EVO spectrometer with an Avalight-XE pulsed xenon light source.

3. Result and discussion

3.1. Structural and phase analysis

3.1.1. X-ray Diffraction (XRD) analysis of membranes. The phase composition of the synthesized membranes was analyzed using X-ray diffraction (XRD). Fig. 1 presents the XRD patterns of the pristine membrane (M-IN) and those containing 1 wt. % (M-1 % CN) and 5 wt. % (M-5 % CN) of powder graphitic carbon nitride (g-C_3N_4). The XRD patterns of all membranes exhibit two prominent diffraction peaks at $2\theta \approx 17^\circ$ and 39°, which are attributed to the characteristic perfluorocarbon chains within the polymer matrix, in agreement with previously reported data [29, 30].

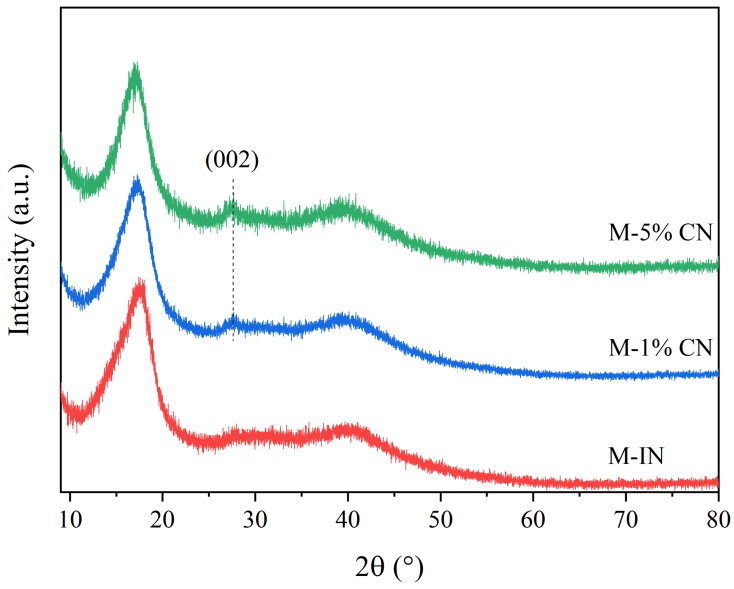

FIG. 1. X-ray diffraction (XRD) patterns of membranes with different g-C_3N_4 filler contents

Upon the incorporation of g-C_3N_4, a new diffraction peak appears at $2\theta \approx 27^\circ$, corresponding to the (002) plane of g-C_3N_4, which is associated with the interlayer stacking of conjugated aromatic rings within its structure [31, 32]. The (100) reflection of g-C_3N_4, typically observed at $2\theta \approx 12.8^\circ$, is not visible due to overlapping reflections from the polymer matrix. The reference XRD pattern of powder g-C_3N_4 and the standard *JCPDS#87-1526* card are provided in Fig. A1 (Appendix).

As shown in Fig. 1, an increase in g-C_3N_4 content results in a progressive enhancement of the (002) peak intensity, confirming the successful integration of the nanofiller into the membrane structure. Additionally, a slight leftward shift of the most intense peak of the polymer matrix is observed, along with changes in its shape, indicating a reduction in membrane crystallinity. This effect suggests that interactions between the g-C_3N_4 nanosheets and the polymer chains disrupt the packing order of the polymer, leading to a more amorphous structure.

Overall, the XRD results confirm the presence of g-C_3N_4 in the membranes and highlight structural modifications induced by increasing filler content. These findings align with previous studies on polymer-based g-C_3N_4 composites, demonstrating their potential for tunable structural properties [31, 32].

3.1.2. Fourier-Transform Infrared Spectroscopy (FTIR) analysis. Fourier-transform infrared (FTIR) spectroscopy was employed to confirm the incorporation of g-C_3N_4 into the polymer matrix and to identify the functional groups responsible for membrane interactions. Fig. 2 presents the FTIR spectra of the synthesized g-C_3N_4 (CN-IN), the pristine membrane (M-IN), and the membranes containing 1 wt. % (M-1 % CN) and 5 wt. % (M-5 % CN) g-C_3N_4. The reference spectrum of CN-IN aligns with previously reported data, with a detailed spectral interpretation provided in earlier studies [21, 33].

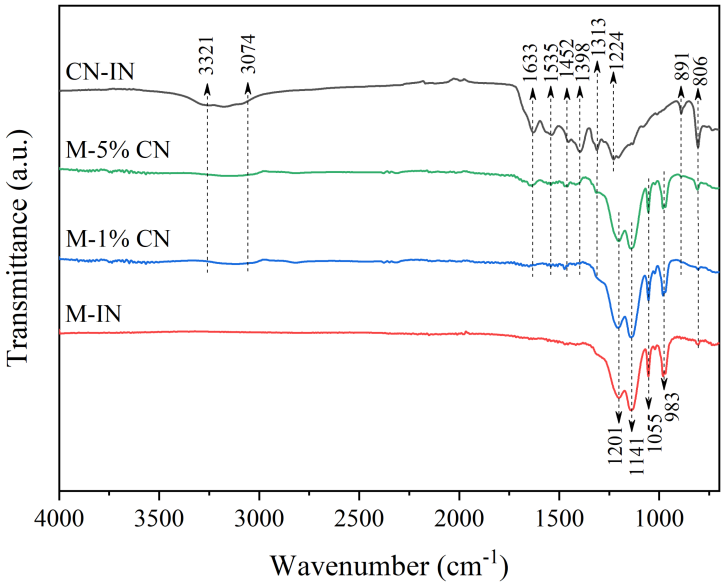

FIG. 2. Fourier-transform infrared (FTIR) spectra of the synthesized g-C_3N_4 and fabricated membranes

The introduction of g-C_3N_4 into the polymer matrix results in an increase in the number of vibration bands observed in the spectra of the modified membranes. This confirms the successful incorporation of the filler into the ionomer structure. A notable change is the emergence of an O–H stretching vibration at 3321 cm^{-1}, which is associated with physically adsorbed water, indicating an increased water retention capacity in g-C_3N_4-containing membranes. Additionally, the presence of characteristic bands for C=N (1535 cm^{-1}), C–N aromatic ring stretching (1224 cm^{-1}), and primary amine (1633 cm^{-1}) groups in the spectra of M-1 % CN and M-5 % CN further supports the incorporation of g-C_3N_4 and its interaction with the polymer matrix.

Furthermore, fluorine-containing functional groups characteristic of the ionomer structure are observed at 1201 and 1141 cm^{-1}, corresponding to asymmetric and symmetric stretching of C–F bonds, respectively. The presence of S–O vibrations at 1055 cm^{-1} confirms the sulfonated nature of the polymer backbone. Additional peaks in the 800 – 1000 cm^{-1} region, particularly at 983 and 891 cm^{-1}, are attributed to ether and aromatic C–H bending vibrations, respectively.

The detailed peak assignments for g-C_3N_4-containing membranes are summarized in Table 1, providing insight into the structural modifications induced by g-C_3N_4 incorporation. These results indicate that the polymer matrix interacts with g-C_3N_4 through hydrogen bonding and electrostatic interactions, leading to changes in membrane hydrophilicity and surface chemistry.

3.2. Morphological and textural properties

3.2.1. Scanning Electron Microscopy (SEM) of membranes. The morphology and microstructure of the synthesized membranes were analyzed using scanning electron microscopy (SEM). Fig. 3(a) presents an optical image of the M-5 % CN membrane, demonstrating its uniform appearance. The surface morphology of the membrane, shown in Fig. 3(b), reveals the presence of evenly distributed nanoparticle agglomerates throughout the polymer matrix, confirming the successful incorporation of g-C_3N_4. This uniform dispersion is essential for maintaining consistent membrane properties and optimizing photocatalytic activity.

Cross-sectional SEM images of the M-5 % CN membrane at different magnifications are displayed in Fig. 3(c–f), providing insights into the internal structure of the membrane. The membrane exhibits a layered architecture with an interconnected network of microscopic pores, which can facilitate ion transport and enhance overall membrane performance. The images in Fig. 3 (c and d) allows for an estimation of the membrane thickness, which is approximately 50 μm, indicating structural integrity suitable for practical applications. At higher magnifications (Fig. 3 (e and f)), the presence of g-C_3N_4 nanosheets embedded within the polymer matrix is observed, contributing to the formation of a well-organized porous structure that may improve adsorption and photocatalytic efficiency.

TABLE 1. FTIR peak assignments for g-C_3N_4-contained membranes

No.	Wavenumber (cm^{-1})	Vibrational Mode	Functional Group Assignment
Hydroxyl & Amine Groups			
1	3321	ν(O–H)	Hydroxyl group (physically adsorbed water)
2	3074	ν(C–H)	Alkenyl C–H stretching
3	1633	ν(N–H)	Primary amine (RNH$_2$)
Carbonyl & Aromatic Functionalities			
4	1535	ν(C=N)	Aromatic C=N in heterocyclic rings
5	1452	δ(CH$_2$)	Aliphatic CH$_2$ bending
6	1398	ν(C–O)	Symmetric and asymmetric carboxylate (RCOO$^-$) stretching
7	1313	ν(C–N)	Tertiary aromatic amines
8	1224	ν(C–N)	C–N stretching in aromatic rings
Fluorine-Containing Functional Groups			
9	1201	ν(C–F, *asym.*)	Asymmetric C–F stretching in fluorinated groups
10	1141	ν(C–F, *sym.*)	Symmetric C–F stretching
Other Characteristic Vibrations			
11	1055	ν(S–O)	Symmetric S–O stretching (sulfonate groups)
12	983	ν(C–O–C)	Ether or alcohol groups
13	891	δ(C–H)	Out-of-plane aromatic C-H bending (3-unsubstituted H atoms)
14	806	δ(C–H)	Out-of-plane aromatic C-H bending (1-unsubstituted H atoms)

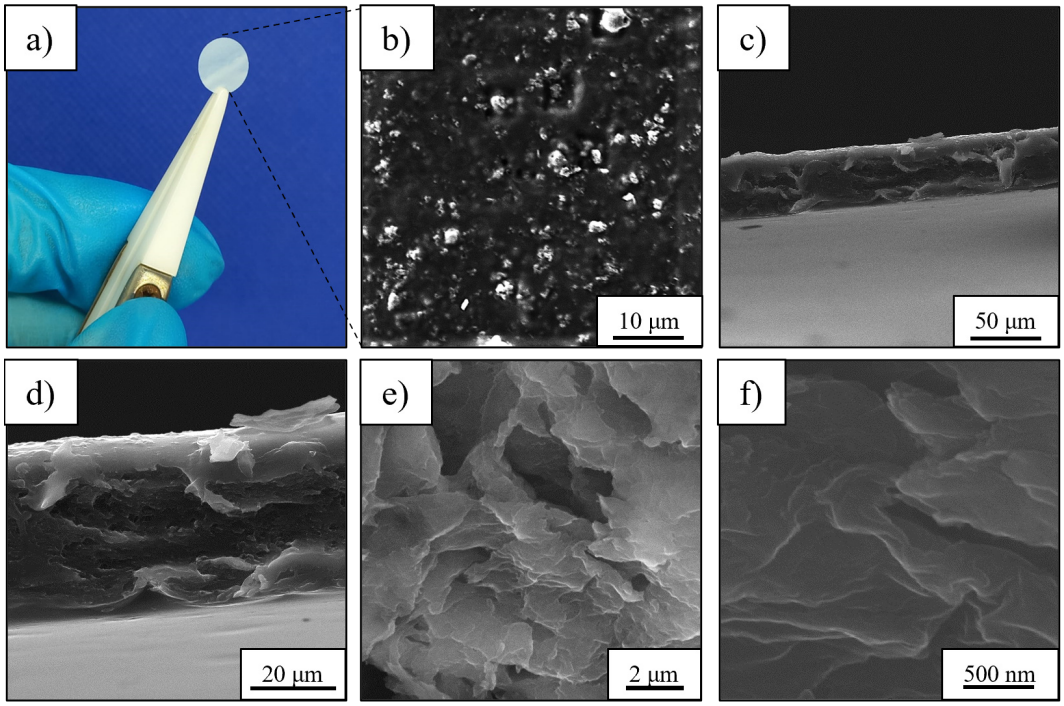

FIG. 3. Morphological analysis of the M-5 % CN membrane: (a) optical image, (b) SEM surface micrograph, (c–f) cross-sectional SEM images at different magnifications

The observed morphological characteristics highlight the potential of the fabricated nanocomposite membranes for water purification applications by providing enhanced surface area, controlled porosity, and efficient charge separation facilitated by the g-C_3N_4 nanofiller. These findings align with previously reported structural features of g-C_3N_4-based polymer composites used in environmental remediation applications [25].

3.2.2. Nitrogen adsorption-desorption isotherm. The textural properties of the g-C_3N_4 powder were analyzed using nitrogen adsorption-desorption isotherms, as presented in Fig. A2 (Appendix). The isotherm exhibits a type IV profile with a well-defined H3 hysteresis loop, which is characteristic of mesoporous materials with slit-shaped pores. The specific surface area (S_{BET}) of the synthesized g-C_3N_4 was determined to be 63 m^2/g, consistent with reported values for powder g-C_3N_4. The pore size distribution, derived from the adsorption branch, further confirms the presence of mesopores in the range of 2–50 nm, which is crucial for enhancing adsorption and charge transfer properties in membrane applications.

As observed in Fig. A2 (Appendix), the adsorption volume increases significantly at high relative pressures ($P/P_0 > 0.8$), indicating the presence of interparticle voids and macroporous structures in the g-C_3N_4 powder. Meanwhile, the gradual rise in adsorption at moderate pressures suggests a contribution from mesopores, which play a key role in improving the dispersion and interaction of g-C_3N_4 within the polymer matrix.

When incorporated into the membrane, the mesoporous nature of g-C_3N_4 is expected to influence the overall textural characteristics. While the pristine membrane (M-IN) exhibits a relatively compact structure, the addition of 5 wt. % g-C_3N_4 is likely to introduce a more heterogeneous porous network. This is particularly beneficial for water purification applications, as the increased porosity can enhance adsorption capacity and facilitate ion transport. These findings confirm that the powder g-C_3N_4 possesses a mesoporous architecture with moderate surface area, which contributes to structural modifications upon integration into the membrane.

3.3. Optical and electronic properties

3.3.1. Diffuse Reflectance UV-Vis Spectroscopy (DRS). The optical properties of the fabricated membranes were analyzed using diffuse reflectance UV-Vis spectroscopy (DRS) to evaluate their light absorption behavior and bandgap energy. Fig. 4(a) presents the reflectance spectra of M-1 % CN and M-5 % CN membranes, revealing their ability to absorb light in the visible region. The presence of the polymer matrix does not induce significant shifts in the optical absorption edge, indicating that the g-C_3N_4 filler retains its intrinsic electronic properties when embedded within the membrane.

To determine the optical bandgap energy (E_g), the Kubelka-Munk function $F(R)$ was applied to the diffuse reflectance data, and the Tauc plot was constructed (inset of Fig. 4(a)). The linear extrapolation of the $[F(R)hv]^2$ vs. hv plot to the *x*-axis yields bandgap values of 2.80 eV for M-1 % CN and 2.86 eV for M-5 % CN, which are consistent with those of pure graphitic carbon nitride (g-C_3N_4). The minor variation in E_g between the two membranes may be attributed to differences in particle dispersion or minor matrix-filler interactions.

These results confirm that the polymer matrix does not significantly alter the optical characteristics of g-C_3N_4, ensuring its photocatalytic functionality in the visible spectrum. The findings highlight the potential of these membranes for photocatalytic water purification applications, where visible-light-driven activation is crucial for pollutant degradation.

3.4. Adsorption performance

3.4.1. Methylene Blue (MB) adsorption studies. The adsorption performance of the fabricated membranes was investigated by monitoring the concentration of methylene blue (MB) over time using UV-Vis spectrophotometry. The adsorption spectra presented in Fig. 4(b) show a gradual decrease in MB absorbance at 664 nm, indicating the progressive adsorption of the dye.

The adsorption kinetics were further analyzed by tracking the relative concentration changes (C/C_0) over time (Fig. 4(c)) and applying a pseudo-second-order kinetic model (Fig. 4(d)). The results demonstrate that the adsorption efficiency significantly improves with increasing g-C_3N_4 content. The M-5 % CN membrane exhibits the highest adsorption rate ($k = 0.08$ min^{-1}), followed by M-1 % CN ($k = 0.063$ min^{-1}), while the pristine membrane (M-IN) shows the lowest adsorption performance ($k = 0.015$ min^{-1}). This enhanced adsorption behavior is attributed to the high surface area of g-C_3N_4 ($S_{BET} = 63$ m^2/g, Fig. A2 (Appendix)), which provides abundant active sites for MB interaction. Additionally, the porous structure of the membranes facilitates dye diffusion, while functional groups on g-C_3N_4 contribute to electrostatic attraction and hydrogen bonding interactions with MB molecules.

These findings confirm that g-C_3N_4 incorporation significantly enhances MB adsorption, making the developed membranes promising candidates for wastewater treatment applications.

3.5. Photocatalytic activity and self-cleaning behavior

3.5.1. Photocatalytic self-cleaning properties of membranes. The photocatalytic performance of the membranes was evaluated through MB degradation under visible-light irradiation ($\lambda = 405$ nm). The degradation kinetics, shown in Fig. 4(e), reveal that MB degradation proceeds more rapidly in membranes containing g-C_3N_4 compared to the pristine membrane (M-IN).

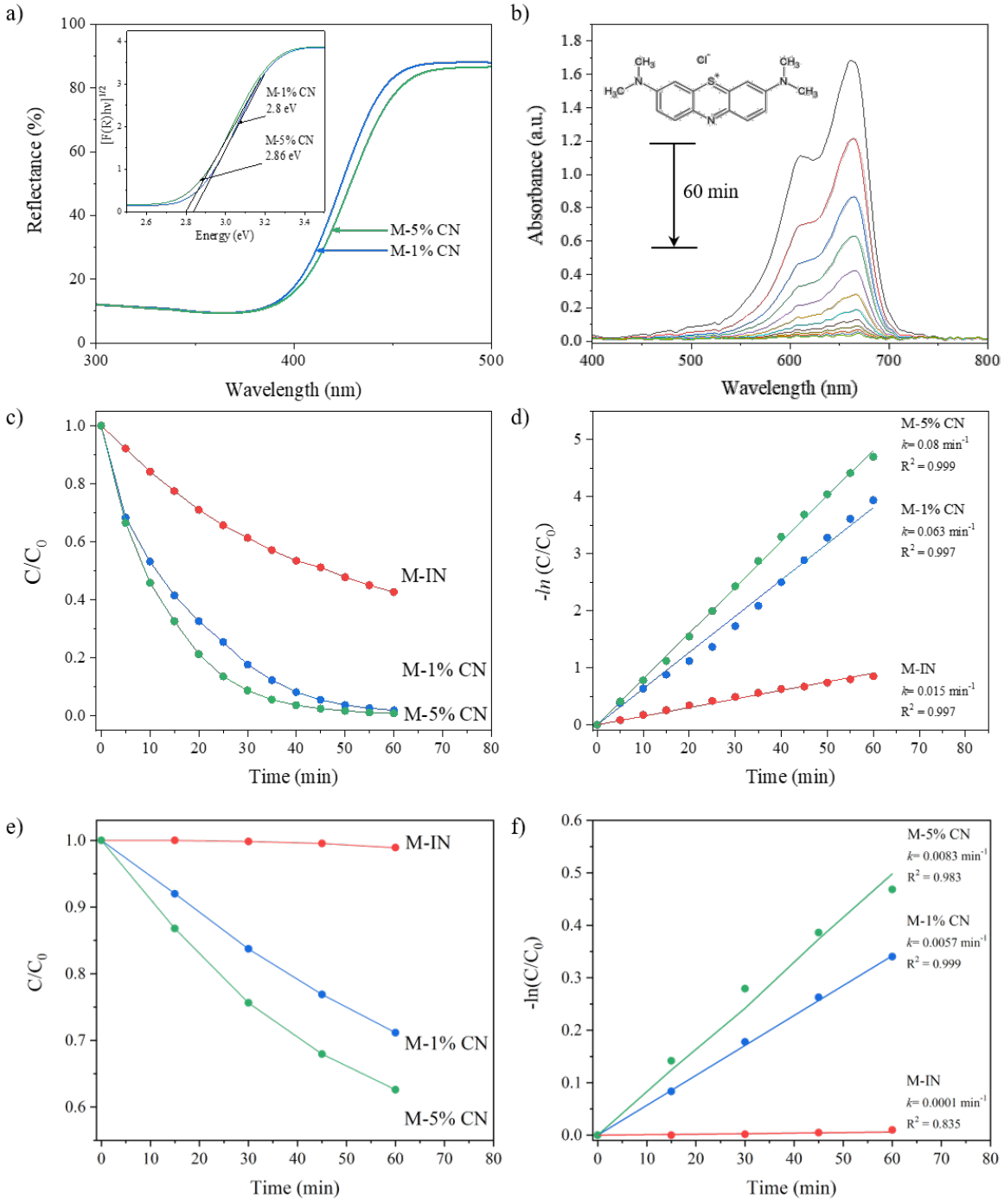

FIG. 4. Optical and adsorption properties of the membranes: (a) diffuse reflectance UV-Vis spectra, (b) adsorption spectra of methylene blue (MB) on the M-5 % CN membrane, (c) relative concentration changes (C/C_0) during MB adsorption, (d) pseudo-second-order kinetics of MB adsorption, (e) photodegradation kinetics of MB under visible light, and (f) corresponding pseudo-first-order kinetic plots

To quantify the degradation kinetics, a pseudo-first-order model was applied (Fig. 4(f)). The reaction rate constants (k) confirm a direct correlation between g-C_3N_4 loading and photocatalytic efficiency, with the highest rate constant observed for M-5 % CN ($k = 0.0083$ min^{-1}), followed by M-1 % CN ($k = 0.0057$ min^{-1}). The pristine M-IN membrane exhibits negligible MB degradation ($k = 0.0001$ min^{-1}), confirming that the polymer matrix alone does not contribute to photocatalysis.

These results highlight the self-cleaning properties of the g-C_3N_4-based membranes, which efficiently degrade organic contaminants under visible-light exposure. The porous architecture facilitates reactant diffusion, while the photocatalytic activity of g-C_3N_4 enables oxidative degradation of MB. These features confirm the potential of g-C_3N_4-modified membranes for antifouling applications in water treatment, providing a sustainable approach to mitigating membrane fouling.

3.6. Comparative performance evaluation

3.6.1. Benchmarking against literature. To evaluate the photocatalytic performance of the synthesized membranes, a comparative analysis was conducted with previously reported photocatalysts capable of absorbing visible light (Table 2). The degradation rate constant (k) of MB for the M-5 % CN membrane obtained in this study (0.0083 min^{-1}) was compared with that of powder g-C_3N_4 (0.0690 min^{-1}) reported in the literature [33], as well as other membranes containing g-C_3N_4 [35, 36].

TABLE 2. Comparative photocatalytic efficiency of synthesized membranes and known photocatalysts in the decomposition of organic pollutants under the influence of visible light

No.	Sample	Organic Pollutants	Rate Constant (min^{-1})	Reference
1	M-5% CN	Methylene Blue	0.0083	This work
2	g-C_3N_4	Methylene Blue	0.0690	[33]
3	g-C_3N_4/PVDF	Phenol	0.0024	[35]
4	MCU-C_3N_4/ PVDF	Rhodamine B TC	0.0074 0.0035	[36]

The results indicate that the M-5 % CN membrane exhibits a competitive photocatalytic degradation rate, comparable to traditional photocatalysts. Importantly, the incorporation of g-C_3N_4 into the polymer matrix does not significantly reduce its photocatalytic efficiency, confirming that the polymer does not act as an inhibitor of photoactivity. Unlike metal-based photocatalysts, g-C_3N_4 is a metal-free material, making it a more environmentally friendly and sustainable alternative. The absence of toxic metal ions enhances its safety profile for practical applications in wastewater treatment.

Overall, the g-C_3N_4-modified membranes combine high photocatalytic performance with the structural advantages of polymeric membranes, such as flexibility, processability, and stability. These findings highlight the potential of M-5 % CN membranes as a promising alternative to conventional metal-based photocatalysts, providing a cost-effective, sustainable, and scalable solution for photocatalytic water purification applications.

4. Conclusion

This study presents the development and characterization of self-cleaning nanocomposite membranes based on sulfonated tetrafluoroethylene and graphitic carbon nitride (g-C_3N_4) for efficient water purification. The membranes were synthesized via a solution casting method, incorporating 1 and 5 wt. % g-C_3N_4 as a photocatalytic filler. Comprehensive structural, morphological, and optical analyses confirmed the successful integration of g-C_3N_4 into the polymer matrix, leading to modifications in crystallinity, surface chemistry, and porosity.

The adsorption and photocatalytic performance of the membranes were evaluated using methylene blue (MB) as a model pollutant. The results demonstrated that increasing the g-C_3N_4 content enhances both adsorption capacity and photocatalytic degradation efficiency under visible-light irradiation. The M-5 % CN membrane exhibited the highest adsorption rate and photocatalytic activity, achieving a MB degradation rate constant of 0.0083 min^{-1}, comparable to or exceeding conventional photocatalysts. The integration of g-C_3N_4 not only retained its intrinsic photocatalytic properties but also conferred antifouling and self-cleaning functionalities to the membranes, highlighting their potential for long-term operation in wastewater treatment applications.

A comparative performance evaluation against reported photocatalytic materials confirmed the competitive efficiency of the developed membranes. Importantly, g-C_3N_4 is a metal-free, environmentally friendly, and scalable material, making it a viable alternative to traditional metal-based photocatalysts. The findings of this study suggest that g-C_3N_4-based

membranes offer a cost-effective and sustainable solution for advanced water purification, combining adsorption, photocatalysis, and self-cleaning properties in a single platform. Future research should focus on optimizing membrane fabrication parameters, exploring long-term stability, and assessing real wastewater treatment performance to further advance their practical applicability.

Appendix

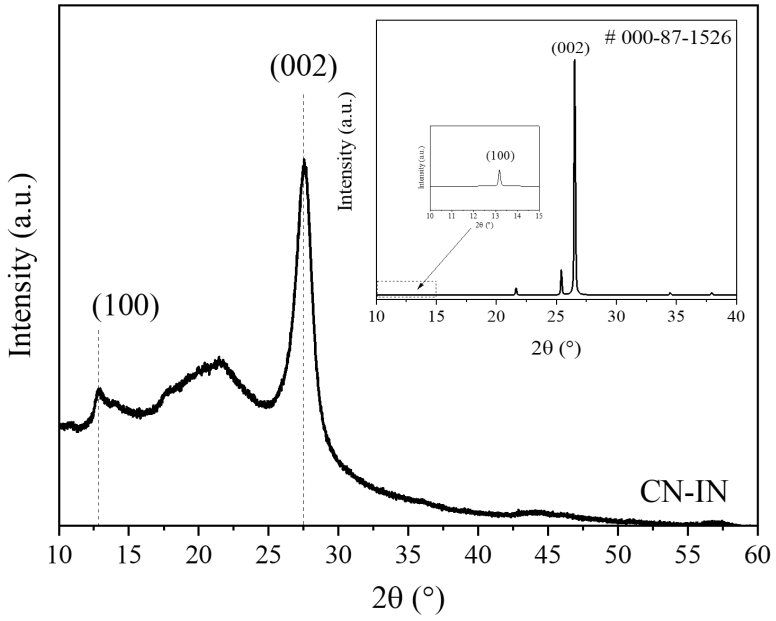

FIG. A1. XRD pattern of the synthesized g-C_3N_4 with a reference *JCPDS#87-1526* pattern (inset)

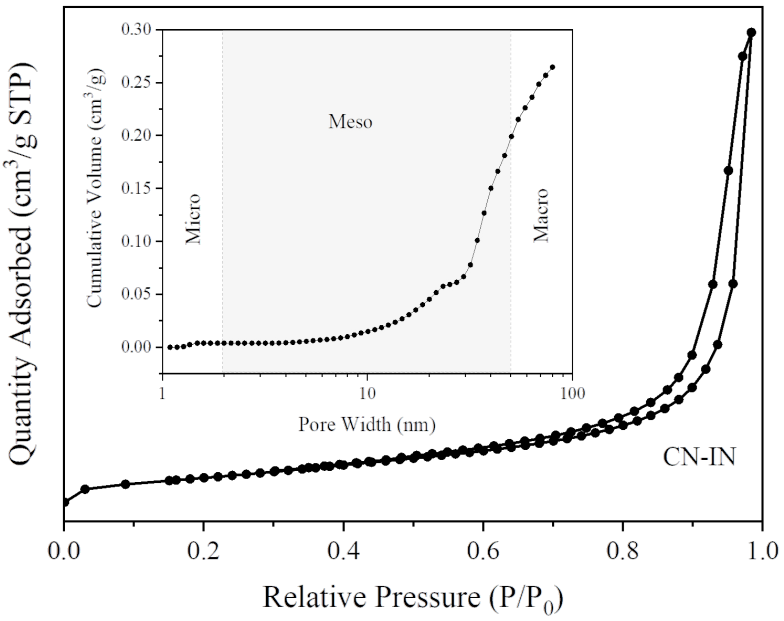

FIG. A2. Nitrogen adsorption-desorption isotherm and pore size distribution of powder g-C_3N_4

References

[1] Wan Nafi A., Taseidifar M. Removal of hazardous ions from aqueous solutions: Current methods, with a focus on green ion flotation. *J. Environ. Manage.*, 2022, **319**, 115666.

[2] Khadhraoui M., Trabelsi H., Ksibi M., Bouguerra S., Elleuch B. Discoloration and detoxicification of a Congo Red dye solution by means of ozone treatment for a possible water reuse. *J. Hazard. Mater.*, 2008, **161**, P. 974–981.

[3] Milena R. Sorption of dyes from aqueous solutions onto fly ash. *Water Res.*, 2018, **37**, P. 4938–4944

[4] Karthikeyan J. Adsorptive removal of direct azo dye from aqueous phase onto coal-based sorbents: A kinetic and mechanistic study. *J. Hazard. Mater.*, 2002, **3894**, P. 189–204.

[5] Bracamontes-Ruelas A.R., Ordaz-Díaz L.A., Bailón-Salas A.M., Ríos-Saucedo J.C., Reyes-Vidal Y., Reynoso-Cuevas L. Emerging pollutants in wastewater, advanced oxidation processes as an alternative treatment and perspectives. *Processes*, 2022, **10**, P. 1–23.

[6] Sun Y., Zhou S., Chiang P.-C., Shah K.J. Evaluation and optimization of enhanced coagulation process: Water and energy nexus. *Water-Energy Nexus*, 2019, **2**, P. 25–36.

[7] Zahrim A.Y., Tizaoui C., Hilal N. Coagulation with polymers for nanofiltration pre-treatment of highly concentrated dyes: A review. *Desalination*, 2011, **266**, P. 1–16.

[8] Romanovski V., Pilipenko M., Dubina A., Likhavitski V., Volodko S., Moskovskikh D., Romanovskaia E. Optimizing dye wastewater purification: ultrasonic and flotation with ozonation synergy. *Eng. Rep.*, 2024, **6**, e13044.

[9] Kökkılıç O., Mohammadi-Jam S., Chu P., Marion C., Yang Y., Waters K.E. Separation of plastic wastes using froth flotation – An overview. *Adv. Colloid Interface Sci.*, 2022, **308**, 102769.

[10] Lin Q., Ding X.-L., Hou Y.-S., Ali W., Li Z.-C., Han X., Meng Z., Sun Y., Liu Y. Adsorption and separation technologies based on supramolecular macrocycles for water treatment. *Eco-Environment Health*, 2024, **3**, P. 381–391.

[11] Si M., Tio O.O.H. On an adsorption/photocatalytic performance of nanotubular materials. *Nanosyst. Phys. Chem. Math.*, 2018, **9** (3), P. 410–416.

[12] Proskynitopoulou V., Vourros A., Garagounis I., Dimopoulos Toursidis P., Lorentzou S., Zouboulis A., Panopoulos K. Enhancing nutrient and water recovery from liquid digestate: A comparative study of selective electrodialysis and conventional treatment methods. *J. Environ. Chem. Eng.*, 2024, **12**, 112675.

[13] Tamilselvan R., Immanuel Selwynraj A. Enhancing biogas production through photocatalytic pretreatment of rice straw co-digested with cow dung and food waste using a novel g-C_3N_4/SiO_2/bentonite catalyst. *Process Saf. Environ. Prot.*, 2024, **187**, P. 799–809.

[14] Lebedev V.T., Kulvelis Y.V., Odinokov A.S., Primachenko O.N., Kononova S.V., Ivan'kova E.M., Orlova V.A., Yevlampieva N.P., Marinenko E.A., Gofman I.V., Shvidchenko A.V., Peters G.S. Proton-conducting membranes based on Nafion® synthesized using a nanodiamond platform. *J. Membr. Sci. Lett.*, 2024, **4**, 100070.

[15] Wang C., Wu Y., Lu J., Zhao J., Cui J., Wu X., Yan Y., Huo P. Bio-inspired synthesis of photocatalytic nanocomposite membranes based on synergy of Au-TiO2 and polydopamine for the degradation of tetracycline under visible light. *ACS Appl. Mater. Interfaces*, 2017, **9**, P. 23687–23697.

[16] Isaev A.B., Magomedova A.G. Advanced oxidation processes-based emerging technologies for dye wastewater treatment. *Moscow Univ. Chem. Bull.*, 2022, **77**, P. 181–196.

[17] Wang C., Wang Y., Qin H., Lin H., Chhuon K. Application of microfiltration membrane technology in water treatment. *IOP Conf. Ser. Earth Environ. Sci.*, 2020, **571**, 012158.

[18] Shehata N., Egirani D., Olabi A.G., Inayat A., Abdelkareem M.A., Chae K.-J., Sayed E.T. Membrane-based water and wastewater treatment technologies: Issues, current trends, challenges, and role in achieving sustainable development goals, and circular economy. *Chemosphere*, 2023, **320**, 137993.

[19] Chebanenko M.I., Zakharova N.V., Popkov V.I. Synthesis and visible-light photocatalytic activity of graphite-like carbon nitride nanopowders. *Russ. J. Appl. Chem.*, 2020, **93**, P. 494–501.

[20] Kavitha J., Rajalakshmi M., Phani A.R., Padaki M. Pretreatment processes for seawater reverse osmosis desalination systems—A review. *J. Water Process Eng.*, 2019, **32**, 100926.

[21] Lebedev L.A., Chebanenko M.I., Popkov V.I. Solvothermal modification of graphitic C_3N_4 with Ni and Co phthalocyanines: Structural, optoelectronic, and photocatalytic properties. *Mendeleev Commun.*, 2022, **32** (5), P. 317–319.

[22] Chebanenko M.I., Martinson K.D., Matsukevich I.V., Popkov V.I. The effect of MgO additive on the g-C_3N_4 performance in electrochemical reforming of water-ethanol solution. *Nanosyst. Phys. Chem. Math.*, 2020, **11** (4), P. 474–479.

[23] Dong F., Wu L., Sun Y., Fu M., Wu Z., Lee S.C. Efficient synthesis of polymeric g-C_3N_4 layered materials as novel efficient visible light driven photocatalysts. *J. Mater. Chem.*, 2011, **21** (40), P. 15171–15174.

[24] Chebanenko M.I., Lebedev L.A., Tenevich M.I., Stovpiaga E.Yu., Popkov V.I. Planetary grinding's impact on the structure and photocatalytic characteristics of urea-derived g-C_3N_4 nanocrystals. *Nanosyst. Phys. Chem. Math.*, 2023, **14** (6), P. 705–712.

[25] Qamar M.A., Javed M., Shahid S., Shariq M., Fadhali M.M., Ali S.K., Khan M.S. Synthesis and applications of graphitic carbon nitride (g-C_3N_4) based membranes for wastewater treatment: A critical review. *Heliyon*, 2023, **9**, e12685.

[26] Dey T., Naughton D. Cleaning and anti-reflective (AR) hydrophobic coating of glass surface: a review from materials science perspective. *J. Sol-Gel Sci. Technol.*, 2016, **77** (1), P. 1–27.

[27] Mittal T. Self-cleaning smart photocatalytic coatings for water treatment. *Mater. Today Proc.*, 2023, **78**, P. 891–894.

[28] Gubanova G.N., Primachenko O.N., Bugrov A.N., Vylegzhanina M.E., Gofman I.V., Lavrentiev V.K., Ivankova E.N., Vlasova E.N., Kononova S.V. Structural and Morphological Features of Perfluorosulfonic Acid Membranes Doped with Zirconium Dioxide Nanoparticles. *J. Surf. Invest.: X-Ray Synchrotron Neutron Tech.*, 2023, **17** (1), P. 391–403.

[29] Sigwadi R., Dhlamini M.S., Mokrani T., ?emavhola F., Nonjola P.F., Msomi P.F. The proton conductivity and mechanical properties of Nafion®/ZrP nanocomposite membrane. *Heliyon*, 2019, **5**, e02240.

[30] Garaev V., Pavlovica S., Reinholds I., Vaivars G. Mechanical properties and XRD of Nafion modified by 2-hydroxyethylammonium ionic liquids. *IOP Conf. Ser. Mater. Sci. Eng.*, 2013, **49** (1), 012058.

[31] Zhurenok A.V., Larina T.V., Markovskaya D.V., Cherepanova S.V., Mel'gunova E.A., Kozlova E.A. Synthesis of graphitic carbon nitride-based photocatalysts for hydrogen evolution under visible light. *Mendeleev Commun.*, 2021, **31** (2), P. 157–159.

[32] Kharina S.N., Kurenkova A.Y., Saraev A.A., Gerasimov E.Y., Kozlova E.A. Copper-modified g-C_3N_4/TiO_2 nanostructured photocatalysts for H? evolution from glucose aqueous solution. *Nanosyst. Phys. Chem. Math.*, 2024, **15** (3), P. 388–397.

[33] Chebanenko M.I., Lebedev L.A., Ugolkov V.L., Prasolov N.D., Nevedomskiy V.N., Popkov V.I. Chemical and structural changes of g-C_3N_4 through oxidative physical vapor deposition. *Appl. Surf. Sci.*, 2022, **600**, 154079.

[34] Matalkeh M., Nasrallah G.K., Shurrab F.M., Al-Absi E.S., Mohammed W., Elzatahry A., Saoud K.M. Visible light photocatalytic activity of Ag/WO_3 nanoparticles and its antibacterial activity under ambient light and in the dark. *Results Eng.*, 2022, **13**, 100313.

[35] Vilamova Z., Sampaio M.J., Svoboda L., Bednar J., Simonova Z., Dvorsky R., Silva C.G., Faria J.L. Enhancing photocatalytic g-C_3N_4/PVDF membranes through new insights into the preparation methods. *Polymer*, 2024, 127238.

[36] Huang J., Hu J., Shi Y., Zeng G., Cheng W., Yu H., Gu Y., Shi L., Yi K. Evaluation of self-cleaning and photocatalytic properties of modified g-C_3N_4 based PVDF membranes driven by visible light. *J. Colloid Interface Sci.*, 2019, **541**, P. 356–366.

Submitted 12 March 2025; accepted 21 June 2025

Information about the authors:

Maria I. Chebanenko – Ioffe Institute, Politechnicheskaya, 26, St. Petersburg, 194021, Russia; ORCID 0000-0002-1461-579X; m_chebanenko@list.ru

Lev A. Lebedev – Ioffe Institute, Politechnicheskaya, 26, St. Petersburg, 194021, Russia; ORCID 0000-0001-9449-9487; 1595lion@gmail.com

Maksim I. Tenevich – Ioffe Institute, Politechnicheskaya, 26, St. Petersburg, 194021, Russia; ORCID 0000-0003-2003-0672; chwm420@gmail.com

Kirill D. Martinson – Ioffe Institute, Politechnicheskaya, 26, St. Petersburg, 194021, Russia; ORCID 0000-0001-9313-4267; martinsonkirill@mail.ru

Oleg N. Primachenko – Branch of Petersburg Nuclear Physics Institute Named by B. P. Konstantinov of National Research Centre "Kurchatov Institute" – Institute of Macromolecular Compounds, Bolshoy Prospekt of Vasilyevsky Island, 31, St. Petersburg 199004, Russia; ORCID 0000-0003-1637-8537; alex-prima@mail.ru

Svetlana V. Kononova – Branch of Petersburg Nuclear Physics Institute Named by B. P. Konstantinov of National Research Centre "Kurchatov Institute" – Institute of Macromolecular Compounds, Bolshoy Prospekt of Vasilyevsky Island, 31, St. Petersburg 199004, Russia; ORCID 0000-0001-5468-3909; svkononova@list.ru

Vadim I. Popkov – Ioffe Institute, Politechnicheskaya, 26, St. Petersburg, 194021, Russia; ORCID 0000-0002-8450-4278; vadim.i.popkov@mail.ioffe.ru

Conflict of interest: the authors declare no conflict of interest.